CHIN. PHYS. LETT. Vol. 38, No. 8 (2021) 087501

Large Magnetoresistance and Nontrivial Berry Phase in Nb_3Sb Crystals with A15 Structure

Qin Chen(陈琴)[1], Yuxing Zhou(周宇星)[1], Binjie Xu(许彬杰)[1], Zhefeng Lou(娄哲丰)[1], Huancheng Chen(陈奂丞)[1], Shuijin Chen(陈水金)[1], Chunxiang Wu(吴春翔)[1], Jianhua Du(杜建华)[2], Hangdong Wang(王杭栋)[3], Jinhu Yang(杨金虎)[3], and Minghu Fang(方明虎)[1,4*]

[1]*Department of Physics, Zhejiang University, Hangzhou 310027, China*
[2]*Department of Applied Physics, China Jiliang University, Hangzhou 310018, China*
[3]*Department of Physics, Hangzhou Normal University, Hangzhou 310036, China*
[4]*Collaborative Innovation Center of Advanced Microstructure, Nanjing University, Nanjing 210093, China*

(Received 3 May 2021; accepted 28 May 2021; published online 2 August 2021)

Compounds with the A15 structure have attracted extensive attention due to their superconductivity and nontrivial topological band structures. We have successfully grown Nb_3Sb single crystals with the A15 structure and systematically measured the longitudinal resistivity, Hall resistivity and quantum oscillations in magnetization. Similar to other topological trivial/nontrivial semimetals, Nb_3Sb exhibits large magnetoresistance (MR) at low temperatures (717%, 2 K and 9 T), unsaturating quadratic field dependence of MR and up-turn behavior in $\rho_{xx}(T)$ curves under magnetic field, which is considered to result from a perfect hole-electron compensation, as evidenced by the Hall resistivity measurements. The nonzero Berry phase obtained from the de-Hass van Alphen (dHvA) oscillations demonstrates that Nb_3Sb is topologically nontrivial. These results indicate that Nb_3Sb superconductor is also a semimetal with large MR and nontrivial Berry phase. This indicates that Nb_3Sb may be another platform to search for the Majorana zero-energy mode.

DOI: 10.1088/0256-307X/38/8/087501

The recent discovery of extremely large magnetoresistance (XMR) up to 10^6% in nonmagnetic semimetals has inspired tremendous interest in understanding its underlying physical mechanisms and exploring its applications in electronics.[1,2] Several mechanisms have been proposed to explain the XMR found in the topologically nontrivial or trivial nonmagnetic semimetals. One scenario attributes the observed linear field dependent MR such as in Cd_3As_2[3,4] and Na_3Bi[5,6] to nontrivial topology including the linear band dispersion. The classical carrier compensation mechanism was used to explain the non-saturating quadratic dependence of MR such as in WTe_2,[1] lanthanum monopnictides LaPn (Pn = As, Sb, Bi),[7–10] as well as in VAs_2.[11] Another mechanism argues that open-orbit trajectories of charge carriers driven by Lorentz force under magnetic field as a result of non-closed Fermi surface to be responsible for XMR as discussed by Zhang *et al.*[12] and materials such as SiP_2[13] and MoO_2[14] appear to support this picture.

Recently, studies on bulk superconductivity in the materials with topologically nontrivial band structure have drawn a great deal of attention due to the possible realization of the Majorana zero-energy mode (MZM). Many compounds with the A15 structure[15] exhibit high temperature superconductivity, such as Nb_3Al (T_c = 18.7 K), V_3Si (T_c = 16.8 K), Nb_3Ge (T_c = 21.8 K). It has also been suggested that the structure symmetry of A15 compounds with spin-orbit coupling (SOC) gives rise to a gapped crossing near the Fermi level. For example, recent theoretical calculations revealed that A15 superconductors Ta_3Sb, Ta_3Sn, and Ta_3Pb have nontrivial band topology in the bulk band structures and topological surface states arise near the Fermi level.[16,17] In particular, Ta_3Sb hosts an eightfold degenerate Dirac point close to the Fermi level at the high symmetry point.[16] First-principles calculations have shown that the gapped Dirac crossings in A15 compounds may result in giant spin Berry curvature and correspondingly giant intrinsic spin Hall effect.[17] Nb_3Sb with the A15 structure is also a superconductor but with very low T_c = 0.2 K.[18] Early research observed de-Hass van Alphen (dHvA) quantum oscillations and Shubnikov-de Hass (SdH) oscillations under 21 T on Nb_3Sb single crystals.[19,20] Recent theoretical calculations indicate that Nb_3Sb may have nontrivial topology in electronic structures. Gao *et al.*[21] predicted various topological semimetals including Nb_3Sb which is considered to host eightfold degenerate fermions. Zhang *et al.*[22] suggested that Nb_3Sb is a high symmetry point semimetal without SOC taken into consideration, while a topological insulator with SOC. Therefore, we attempt to grow Nb_3Sb single crystals to

Supported by the National Key R&D Program of China (Grant No. 2016YFA0300402), the National Natural Science Foundation of China (Grant Nos. 12074335, and 11974095), and the Fundamental Research Funds for the Central Universities.
*Corresponding author. Email: mhfang@zju.edu.cn

study its topological nature.

In this work, based on the successful synthesis of Nb_3Sb single crystals, we performed comprehensive measurements of longitudinal resistivity, Hall resistivity and the quantum oscillations of magnetization. Our results show that Nb_3Sb has large unsaturated quadratic field dependent MR (717%, 2 K and 9 T) at low temperatures with up-turn behavior similar to other topological nontrivial/trivial semimetals. The Hall resistivity data indicates that Nb_3Sb is a perfect hole-electron compensated semimetal. The nonzero Berry phase obtained from the dHvA quantum oscillation of magnetization demonstrates that Nb_3Sb is topologically nontrivial. These results indicate that the Nb_3Sb may be a promising platform to investigate the relationship between XMR, topology and superconductivity.

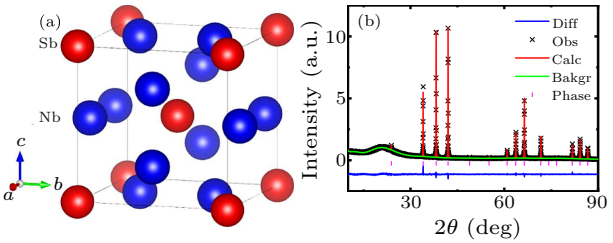

Fig. 1. (a) Crystal structure of the cubic Nb_3Sb. (b) XRD pattern of powder obtained by grinding Nb_3Sb crystals, the line shows its Rietveld refinement.

Experimental Methods and Calculations. Nb_3Sb single crystals were grown by a chemical vapor transport method. Stoichiometrical ratio of high purity Nb powders (99.999%) and Sb powders (99.999%) were sealed in an evacuated quartz tube with 10 mg/cm^3 iodine as a transport agent, then heated for two weeks in a tube furnace with a temperature gradient of 1220–1120 K. Silver grey crystals with typical dimensions $1.0 \times 1.0 \times 0.2\,\text{mm}^3$ were obtained at the cold end of the tube. The composition was confirmed to be Nb:Sb = 3:1 using the energy dispersive x-ray spectrometer (EDXS). The crystal structure was determined by a powder x-ray diffractometer (XRD, PANalytical), created by grinding pieces of crystals [see Fig. 1(b)]. It was confirmed that Nb_3Sb crystallizes in a cubic structure (space group $Pm\bar{3}n$, No. 223). The lattice parameters, $a = b = c = 5.26(2)$ Å were obtained using Rietveld refinement to the XRD data (weighted profile factor $R_{\text{wp}} = 7.62\%$, and the goodness-of-fit $\chi^2 = 2.556$), as shown in Fig. 1(b). Electrical resistivity (ρ_{xx}), Hall resistivity (ρ_{xy}), and magnetization measurements were carried out using a Quantum Design physical property measurement system (PPMS-9T) or Quantum Design magnetic property measurement system (MPMS-7T).

Results and Discussion. Firstly, we discuss the longitudinal resistivity ρ_{xx} of Nb_3Sb measured at various temperatures and in different magnetic fields. The resistivity measured at $\mu_0 H = 0$ T [see Fig. 2(a)] exhibits a metallic behavior with $\rho(2\,\text{K}) = 0.29\,\mu\Omega\cdot\text{cm}$, and $\rho(300\,\text{K}) = 18\,\mu\Omega\cdot\text{cm}$, thus the residual resistivity ratio (RRR) $\rho(300\,\text{K})/\rho(2\,\text{K}) \sim 62$, indicating that the Nb_3Sb crystal has a high quality. It was found that Nb_3Sb crystal exhibits large magnetoresistance. As shown in the inset of Fig. 2(a), an up-turn behavior in $\rho_{xx}(T)$ curves is observed under applied magnetic field at low temperatures: ρ_{xx} increases with decreasing T and then saturates. Figure 2(b) shows MR as a function of temperature at various magnetic fields, with the conventional definition $MR = \frac{\Delta\rho}{\rho(0)} = [\frac{\rho(H)-\rho(0)}{\rho(0)}] \times 100\%$. The normalized MR, shown in the inset of Fig. 2(b), has the same temperature dependence for various fields, excluding the suggestion of a field-induced metal-insulator transition[23,24] at low temperatures, as discussed in our work on the topologically trivial semimetal α-WP_2,[25] and Thoutam *et al.* worked on the type-Ⅱ Weyl semimetal WTe_2.[26]

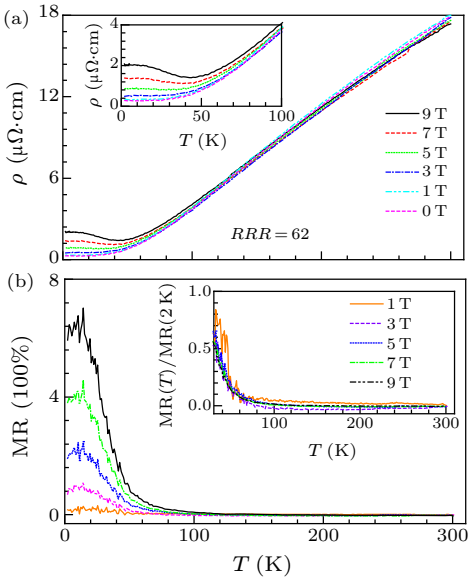

Fig. 2. (a) Temperature dependence of longitudinal resistivity, $\rho_{xx}(T)$, measured at various magnetic fields for a Nb_3Sb crystal. The inset shows the low temperature data. (b) The MR as a function of temperature measured at various magnetic fields. The inset shows the temperature dependence of MR normalized by its value at 2 K at various magnetic fields.

Figure 3(a) shows the MR as a function of field at different temperatures. The measured MR is large at low temperatures, reaching 717% at 2 K and 9 T, and having no sign of saturation up to the highest field (9 T) applied in our measurements. In addition, MR can be described by the Kohler scaling law[27]

$$\text{MR} = \frac{\Delta\rho_{xx}(T,H)}{\rho_0(T)} = \alpha(H/\rho_0)^m. \quad (1)$$

As shown in Fig. 3(b), all the MR data measured from $T = 2$ to 100 K collapse onto a single straight

line when plotted as MR $\sim H/\rho_0$ curve, with $\alpha = 0.026\,(\mu\Omega\cdot\mathrm{cm/T})^{1.8}$ and $m = 1.8$ obtained by fitting. The nearly quadratic field dependence of MR observed for this semimetal Nb_3Sb is attributed to the perfect electron-hole compensation, as evidenced by the Hall resistivity measurements discussed below, which is a common characteristic for most of the topologically nontrivial and trivial semimetals.[25,28,29]

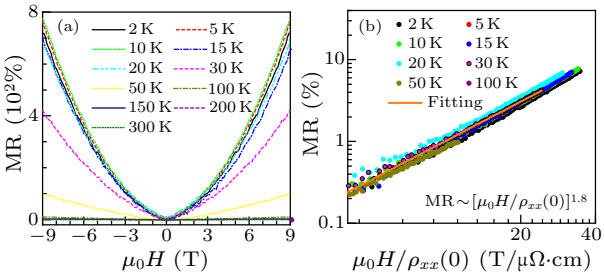

Fig. 3. (a) Field dependence of MR at various temperatures. (b) MR as a function of $H/\rho_{xx}(0)$ plotted on a log scale.

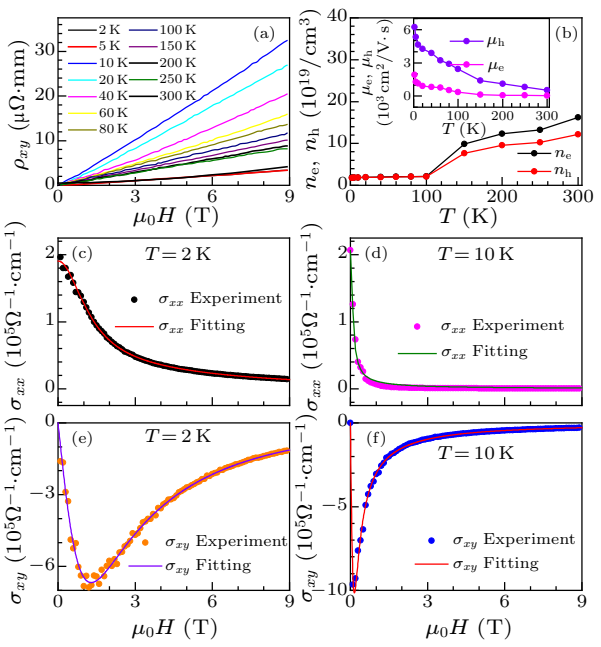

Fig. 4. (a) Field dependence of Hall resistivity ρ_{xy} at different temperatures for a Nb_3Sb crystal. (b) The carrier concentrations, n_e and n_h, and (inset) charge-carrier mobilities, μ_e and μ_h, versus temperature extracted from the two-carrier model. Components of the conductivity tensor, i.e., σ_{xx} and σ_{xy} in panels (c), (d), (e) and (f), respectively, as functions of magnetic field for temperatures at 2 K and 10 K. Dots represent experimental data and solid lines the fitting curves based on the two-carrier model.

We then discuss the characteristics of charge carriers in Nb_3Sb relying on the Hall resistivity measurements. Figure 4(a) displays $\rho_{xy}(H)$ measured at various temperatures. Although the linear dependence of $\rho_{xy}(H)$ with a positive slope indicates that the holes dominate the transport properties, it is not true for a semimetal, in which both electron and hole carriers coexist, as discussed by us for the MoO_2.[14] Following the analysis of γ-$MoTe_2$ by Zhou *et al.*,[30] as well as for MoO_2 by ourselves,[14] we analyzed the longitudinal and Hall resistivity data using the semiclassical two-carrier model. In this model, the conductivity tensor, in the complex representation, is given by[1]

$$\sigma = \frac{en_e\mu_e}{1+i\mu_e\mu_0 H} + \frac{en_h\mu_h}{1-i\mu_h\mu_0 H}, \tag{2}$$

where n_e and n_h denote the electron and hole concentrations, μ_e and μ_h denote the mobilities of electrons and holes, respectively. From Eq. (2), the Hall conductivity σ_{xy} is the imaginary part and the longitudinal conductivity σ_{xx} is the real part expressed as follows:[30]

$$\sigma_{xy} = \frac{e\mu_0 H n_h\mu_h^2}{1+\mu_h^2\mu_0^2H^2} - \frac{e\mu_0 H n_e\mu_e^2}{1+\mu_e^2\mu_0^2H^2}, \tag{3}$$

$$\sigma_{xx} = \frac{en_h\mu_h}{1+\mu_h^2\mu_0^2H^2} + \frac{en_e\mu_e}{1+\mu_e^2\mu_0^2H^2}. \tag{4}$$

To appropriately evaluate the carrier densities and mobilities, we calculate the Hall conductivity $\sigma_{xy} = -\rho_{xy}/(\rho_{xx}^2+\rho_{xy}^2)$ and the longitudinal conductivity $\sigma_{xx} = \rho_{xx}/(\rho_{xx}^2+\rho_{xy}^2)$ using the experimentally observed Hall resistivity $\rho_{xy}(H)$ and longitudinal resistivity $\rho_{xx}(H)$. We then fit both $\sigma_{xy}(H)$ and $\sigma_{xx}(H)$ data using Eqs. (3) and (4).

Figures 4(c)–4(f) display the fits of both the $\sigma_{xx}(H)$ and $\sigma_{xy}(H)$ at $T = 2$ K and 10 K, respectively. The excellent agreement between our experimental data and the two-carrier model over a broad range of temperatures confirms the coexistence of electrons and holes in Nb_3Sb. Figure 4(b) shows the n_e, n_h, μ_e and μ_h values obtained by the fitting over the temperature range 2–300 K. It is remarkable that the n_e and n_h values are almost the same below 100 K, such as at 2 K, $n_e = 1.83\times10^{19}\,\mathrm{cm}^{-3}$, and $n_h = 1.79\times10^{19}\,\mathrm{cm}^{-3}$. These results indicate that the MR in Nb_3Sb semimetal indeed results from the perfect compensation of the two kinds of charge carriers, similar to those observed in many trivial and nontrivial topological semimetals.[1,31–35] Due to the existence of phonon thermal scattering at higher temperatures, as shown in the inset of Fig. 4(b), it is obvious that both μ_e and μ_h decrease notably with increasing temperature. It is worth noting that hole mobility μ_h is larger than μ_e at lower temperatures, such as at 2 K, $\mu_h = 6.2\times10^3\,\mathrm{cm}^2/\mathrm{V\cdot s}$, and $\mu_e = 1.9\times10^3\,\mathrm{cm}^2/\mathrm{V\cdot s}$.

Finally, to obtain additional information on the electronic structure, we measured the dHvA quantum oscillations in the isothermal magnetization, $M(H)$, for a Nb_3Sb crystal up to 7 T for the $H \parallel c$ axis orientation. After subtracting a smooth background from the $M(H)$ data at each temperature, the periodic oscillations are visible in $1/H$, as shown in Fig. 5(a). From the fast Fourier transformation (FFT) analysis, we derived four basic frequencies [Fig. 5(b)].

In general, the oscillatory magnetization of three-dimensional (3D) systems can be described by the the Lifshitz–Kosevich (LK) formula[36,37] with the Berry phase:[38]

$$\Delta M \propto -B^{1/2} R_{\rm T} R_{\rm D} R_{\rm S} \sin[2\pi(F/B - \gamma - \delta)], \quad (5)$$

$$R_{\rm T} = \alpha T\mu/B \sinh(\alpha T\mu/B), \quad (6)$$

$$R_{\rm D} = \exp(-\alpha T_{\rm D}\mu/B), \quad (7)$$

$$R_{\rm S} = \cos(\pi g\mu/2), \quad (8)$$

where μ is the ratio of effective cyclotron mass m^* to free electron mass m_0. T_D is the Dingle temperature, and $\alpha = (2\pi^2 k_{\rm B} m_0)/(\hbar e)$. The phase factor $\delta = 1/8$ or $-1/8$ for three dimensional system. The effective mass m^* can be obtained by fitting the temperature dependence of the oscillation amplitude $R_{\rm T}(T)$, as shown in Fig. 5(c). For $F_\beta = 79\,{\rm T}$, the obtained m^* is $0.17m_0$. Using the fitted m^* as a known parameter, we can further fit the oscillation patterns at a given temperatures [e.g., $T = 2\,{\rm K}$, see Fig. 5(d)] to the LK formula with the frequency, from which quantum mobility and the Berry phase $\phi_{\rm B}$ can be extracted. The fitted Dingle temperature T_D is of 8.0 K, which corresponds to the quantum relaxation time $\tau_q = \hbar/(2\pi k_{\rm B} T_D)$ being of 0.15 ps, and quantum mobility $\mu_q = e\tau/m^*$ being of 1551 $\rm cm^2/V{\cdot}s$. The LK fit also yields a phase factor $-\gamma-\delta$ of 0.82, in which $\gamma = \frac{1}{2} - \frac{\phi_{\rm B}}{2\pi}$ and the Berry phase $\phi_{\rm B}$ is determined to be 0.89π for $\delta = 1/8$ and 0.39π for $\delta = -1/8$. As is well known, topological nontrivial materials require a nontrivial π Berry phase; while for the trivial materials, the Berry phase equals 0 or 2π. In our sample, the Berry phase is close to the π, so it is a topological nontrivial materials. The results for the other frequencies are listed in Table 1.

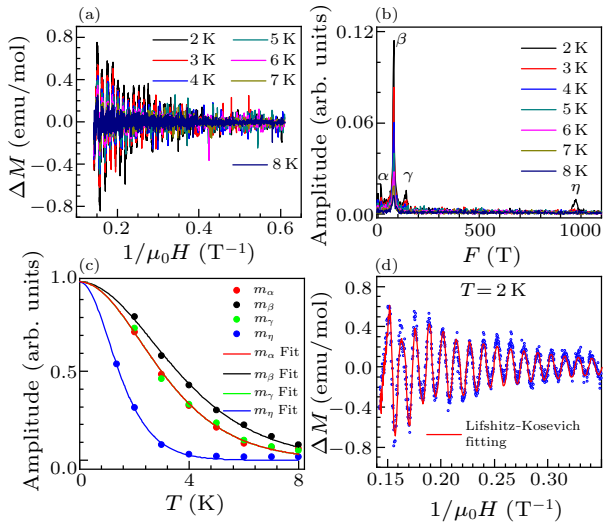

Fig. 5. (a) The amplitude of dHvA plotted as a function of $1/\mu_0 H$. (b) FFT spectra of the oscillations between 2 K and 8 K. (c) The temperature dependence of relative FFT amplitude of frequency and the fitting result by $R_{\rm T}$. (d) The fitting of dHvA oscillations at 2 K by the multi-band LK formula.

Table 1. The obtained parameters by fitting dHvA data for Nb_3Sb.

Parameters	F_α	F_β	F_γ	F_η
Frequency (T)	15	79	139	970
m^*/m_0	0.21	0.17	0.21	0.41
$T_{\rm D}$ (K)	5.2	8.0	4.1	9.0
$\tau_{\rm q}$ (ps)	0.23	0.15	0.30	0.13
$\mu_{\rm q}$ ($\rm cm^2/V{\cdot}s$)	1925	1511	2512	5574
$\phi_{\rm B}(\delta{=}+1/8)$	0.65π	0.89π	0.19π	0.49π
$\phi_{\rm B}(\delta=-1/8)$	0.15π	0.39π	0.69π	1.99π

In summary, Nb_3Sb with the A15 structure have been studied in detail by longitudinal resistivity, Hall resistivity, and dHvA oscillations in magnetization measurements. It is found that the MR exhibits a field induced up-turn behavior with unsaturated $H^{1.8}$ dependence, which is believed to arise from the carrier compensation, as evidenced by the Hall resistivity results. We also obtain the nonzero Berry phase from the dHvA oscillations, indicating the nontrivial topology of band structure in Nb_3Sb. Therefore, it is vital to study the topological nature of Nb_3Sb in superconducting state in future studies.

References

[1] Ali M N, Xiong J, Flynn S, Tao J, Gibson Q D, Schoop L M, Liang T, Haldolaarachchige N, Hirschberger M, Ong N P and Cava R J 2014 *Nature* **514** 205

[2] Tafti F F, Gibson Q, Kushwaha S, Krizan J W, Haldolaarachchige N and Cava R J 2016 *Proc. Natl. Acad. Sci. USA* **113** E3475

[3] He L P, Hong X C, Dong J K, Pan J, Zhang Z, Zhang J and Li S Y 2014 *Phys. Rev. Lett.* **113** 246402

[4] Liang T, Gibson Q, Ali M N, Liu M, Cava R and Ong N 2015 *Nat. Mater.* **14** 280

[5] Wang Z, Sun Y, Chen X Q, Franchini C, Xu G, Weng H, Dai X and Fang Z 2012 *Phys. Rev. B* **85** 195320

[6] Xiong J, Kushwaha S K, Liang T, Krizan J W, Hirschberger M, Wang W, Cava R and Ong N 2015 *Science* **350** 413

[7] Guo P J, Yang H C, Zhang B J, Liu K and Lu Z Y 2016 *Phys. Rev. B* **93** 235142

[8] Zeng L K, Lou R, Wu D S, Xu Q N, Guo P J, Kong L Y, Zhong Y G, Ma J Z, Fu B B, Richard P, Wang P, Liu G T, Lu L, Huang Y B, Fang C, Sun S S, Wang Q, Wang L, Shi Y G, Weng H M, Lei H C, Liu K, Wang S C, Qian T, Luo J L and Ding H 2016 *Phys. Rev. Lett.* **117** 127204

[9] Niu X H, Xu D F, Bai Y H, Song Q, Shen X P, Xie B P, Sun Z, Huang Y B, Peets D C and Feng D L 2016 *Phys. Rev. B* **94** 165163

[10] Yang H Y, Nummy T, Li H, Jaszewski S, Abramchuk M, Dessau D S and Tafti F 2017 *Phys. Rev. B* **96** 235128

[11] Chen S, Lou Z, Zhou Y, Chen Q, Xu B, Wu C, Du J, Yang J, Wang H and Fang M 2021 *Chin. Phys. Lett.* **38** 017202

[12] Zhang S, Wu Q, Liu Y and Yazyev O V 2019 *Phys. Rev. B* **99** 035142

[13] Zhou Y, Lou Z, Zhang S, Chen H, Chen Q, Xu B, Du J, Yang J, Wang H, Xi C, Pi L, Wu Q, Yazyev O V and Fang M 2020 *Phys. Rev. B* **102** 115145

[14] Chen Q, Lou Z, Zhang S, Xu B, Zhou Y, Chen H, Chen S, Du J, Wang H, Yang J, Wu Q, Yazyev O V and Fang M 2020 *Phys. Rev. B* **102** 165133

[15] Stewart G 2015 *Physica C* **514** 28

[16] Kim M, Wang C Z and Ho K M 2019 *Phys. Rev. B* **99** 224506

[17] Derunova E, Sun Y, Felser C, Parkin S, Yan B and Ali M

2019 *Sci. Adv.* **5** eaav8575
[18] Knapp G S, Bader S D and Fisk Z 1976 *Phys. Rev. B* **13** 3783
[19] Arko A, Fisk Z and Mueller F 1977 *Phys. Rev. B* **16** 1387
[20] Sellmyer D, Liebowitz D, Arko A and Fisk Z 1980 *J. Low Temp. Phys.* **40** 629
[21] Gao H, Venderbos J W, Kim Y and Rappe A M 2019 *Annu. Rev. Mater. Res.* **49** 153
[22] Zhang T, Jiang Y, Song Z, Huang H, He Y, Fang Z, Weng H and Fang C 2019 *Nature* **566** 475
[23] Zhao Y, Liu H, Yan J, An W, Liu J, Zhang X, Wang H, Liu Y, Jiang H and Li Q 2015 *Phys. Rev. B* **92** 041104
[24] Khveshchenko D 2001 *Phys. Rev. Lett.* **87** 206401
[25] Du J, Lou Z, Zhang S *et al.* 2018 *Phys. Rev. B* **97** 245101
[26] Thoutam L, Wang Y, Xiao Z, Das S, Luican-Mayer A, Divan R, Crabtree G and Kwok W 2015 *Phys. Rev. Lett.* **115** 046602
[27] Pippard A B 1989 *Magnetoresistance in Metals* (New York: Cambridge University Press)
[28] Wang A, Graf D, Liu Y *et al.* 2017 *Phys. Rev. B* **96** 121107
[29] Chen B, Duan X, Wang H *et al.* 2018 *npj Quantum Mater.* **3** 1
[30] Zhou Q, Rhodes D, Zhang Q, Tang S, Schönemann R and Balicas L 2016 *Phys. Rev. B* **94** 121101
[31] Takatsu H, Ishikawa J J, Yonezawa S, Yoshino H, Shishidou T, Oguchi T, Murata K and Maeno Y 2013 *Phys. Rev. Lett.* **111** 056601
[32] Mun E, Ko H, Miller G J, Samolyuk G D, Bud'Ko S L and Canfield P C 2012 *Phys. Rev. B* **85** 035135
[33] Yuan Z, Lu H, Liu Y, Wang J and Jia S 2016 *Phys. Rev. B* **93** 184405
[34] Huang X, Zhao L, Long Y *et al.* 2015 *Phys. Rev. X* **5** 031023
[35] Chen F, Lv H, Luo X, Lu W, Pei Q, Lin G, Han Y, Zhu X, Song W and Sun Y 2016 *Phys. Rev. B* **94** 235154
[36] Lifshitz I and Kosevich A 1956 *Sov. Phys. JETP* **2** 636
[37] Shoenberg D 2009 *Magnetic Quantum Oscillations* (Cambridge: Cambridge University Press)
[38] Mikitik G and Sharlai Y V 1999 *Phys. Rev. Lett.* **82** 2147